COBEM 2021 26th International Congress of Mechanical Engineering
ABCM Associação Brasileira de Engenharia e Ciências Mecânicas
November 22-26, 2021, Virtual Congress, Brazil

COB-2021-2113
THERMODYNAMIC MODELING OF A HYBRID PLANT CONSIDERING SOLAR THERMAL ENERGY AND COMBINED POWER CYCLE

Bernardo Bergantini Botamede[1]
Leandro de Oliveira Salviano[2]
São Paulo State University, Engineering College at Ilha Solteira. Av. Brasil, 56 - Centro - Ilha Solteira/SP - CEP 15385-000
[1] b.botamede@unesp.br, [2] leandro.salviano@unesp.br

Abstract. *Solar Thermal Energy is currently used for power generation as a reliable carbon-free source in many countries. Unfortunately, there is no such commercial project under operation in Brazil, although a great solar potential is verified. In this context, an interesting strategy to transition is to develop a hybrid solar plant that can be applied on current thermoelectric power plants. Therefore, the present work investigates some layout alternatives for coupling a solar thermal plant with an operational plant base on a combined cycle (Brayton and Rankine cycle) located in Brazil. A parabolic trough collector was selected for this study, considering oil and molten salt as working fluids. The thermodynamic modeling and additional mathematical models were developed on the open-source software OpenModelica. The thermodynamic modeling of the current power plant model was validated through real operating data, kindly provided by a private company. Moreover, a typical concentrate solar plant with thermal storage was modeled and validated through reference software called System Advisor Model (SAM) from National Renewable Energy Laboratory (NREL) in the USA. A proposed solar plant with thermal storage is integrated into Heat Recovery Steam Generator (HRSG) considering several layouts for different strategies either to supply heated water, saturated or superheated steam. Results showed the layouts that use solar energy to superheat saturated steam have the best thermodynamic performance, with solar-to-electric convertion efficiency up to 47.21%, and 1.42% increase in average daily steam turbine gross power under nominal Direct Normal Irradiance (DNI) conditions.*

Keywords: *Thermodynamic modeling, Solar Thermal Energy, Parabolic Trough Collector, Hybrid Power Plant.*

1. INTRODUCTION

Solar Thermal Energy is currently used for electric power generation as a reliable carbon-free source in many countries. Unfortunately, there is no such commercial project under operation in Brazil, although a great solar potential is verified. In this context, hybridization with other primary resources has been proposed as an economical alternative and a transition strategy to boost solar thermal into new markets (Peterseim et al. 2014; Powell et al. 2017).

Natural gas combined cycle (NGCC) plants are an attractive option for solar hybridization in Brazil, considering the extensive natural gas reserves available and the presence of numerous power plants in locations with high solar incidence. Natural gas has also a much lower carbon emission and reduced environmental impacts when compared to other fossil fuels. Moreover, NGCC power plants are fundamental for short and long-term stability of the National Interconnected System (SIN), especially for a future scenario where more intermittent renewable sources will be deployed. Diverse resources from NGCC plants can be shared with solar plants, such as turbomachinery, pumps, heat rejection systems, water supply, and others, thus enabling the optimization of capital and operational expenditures (CAPEX & OPEX) and reduction of levelized cost of solar thermal energy (LCOE).

Several hybrid configurations and strategies were proposed in the literature, considering solar integration both on topping cycle (Brayton cycle) and bottoming cycle (Rankine cycle) (Powell et al. 2017; Pramanik and Ravikrishna 2017). Behar (Behar 2018) evaluated the thermal performance of fifteen fossil, hybrid and solar plants, and results showed that the most effective option for solar energy conversion is the integration of the parabolic trough solar field with synthetic oil on the bottoming cycle. Manente et al. (Manente, Rech, and Lazzaretto 2016) analyzed selected layouts for solar integration on a three pressure level bottoming cycle (NGCC), considering parabolic trough, linear fresnel and solar tower, and concluded that parabolic trough with synthetic oil applied for evaporating high pressure saturated water presented the highest value of the solar thermal-to-electrical efficiency. Elmohlawy (Elmohlawy, Ochkov, and Kazandzhan 2019) investigated two layouts for coupling solar with high and intermediate pressure levels of a NGCC plant, considering parabolic trough and synthetic oil. Injection of superheated steam on high-pressure level achieved 62.95% efficiency against 61.75% on the intermediate pressure level. In general, recent projects under development adopt bottoming cycle integration with parabolic trough collectors, with solar share from 3% up to 14% from total power output.

The retrofit of an operating plant for solar hybridization, however, should consider technical restrictions and possible bottlenecks of each project and equipment, as well as local market conditions and regulatory aspects that have a stark influence over technical and economic analysis. From this perspective, some recent works were performed to evaluate the potential for coupling solar with existing NGCC plants on different markets. Antonanzas et al. (Antonanzas et al. 2015) performed a feasibility study of the potential for solar thermal hybridization in Algerian open cycle gas turbines and combined cycle gas turbines. Boretti and Al-Zubaidy (Boretti and Al-Zubaidy 2019) evaluated the potential for coupling a solar plant with no thermal storage with an existing NGCC plant located in Trinidad y Tobago. Abdelhalim and Suárez (Abdelhalim and Suárez-Ramón 2020) investigate the potential for fuel savings using solar hybridization in a combined cycle plant in Egypt. All these works consider parabolic trough technology and minor modifications on the base plant, although the upgrade of some key components is also a possibility to enable a higher solar share. Manente (Manente 2016) evaluated different schemes for coupling solar energy with a three-pressure level 390 MWe natural gas combined cycle located in Italy, either by keeping the same combined cycle equipments or by upgrading the steam turbine and the Heat Recovery Steam Generator (HRSG). Keeping the equipments unchanged, the solar energy fraction is limited to 19 MWe for saving fuel strategy and 17 MWe for power-boosting mode, while 50 MWe or more from solar could be obtained by replacing the existing equipments.

Integration of solar with other renewables sources in the Brazilian scenario was accessed by some authors. Burin et al. (E. K. Burin et al. 2015, 2016) investigated layout alternatives for coupling solar with a sugarcane bagasse cogeneration plant. Hybridization enabled fuel economy and extended electric generation over the off-season period, increasing the plant's capacity factor. Integration of linear Fresnel collectors with a cogeneration cycle on a paper mill plant was also proposed for providing additional electric output (E. Burin, Giudice, and Bazzo 2018). Soria et al. (Soria et al. 2015) evaluated solar power coupled with biomass plants on semiarid and evaluated some policy implications for deployment of CSP in Brazil.

No studies were found regarding to the thermodynamic modeling of an existing NGCC plant in the Brazilian energy market considering solar thermal energy hybridization. Therefore, the present work investigates some layout alternatives for coupling solar thermal plant with an operational plant based on combined cycle (Brayton and Rankine cycle) located in Brazil, considering parabolic trough collectors as the concentrating technology, and synthetic oil or molten salt as working fluids. The thermodynamic modeling and additional mathematical models were developed on the open source software OpenModelica. One dimensional (1-D) dynamic mathematical model was used for modeling the trough collector receiver and internal flow on each section of Heat Recovery Steam Generator (HRSG). Conduction, convection and radiation heat transfer was modeled on receiver tube, glass cover and brackets. Constant isentropic efficiency was adopted for pumps, gas and steam turbines, and the heat exchangers in the solar plant were modeled by means of Number of Transfer Units method (NTU). A thermal energy storage (TES) system was modeled as two tank system with both direct or indirect storage, and a TES dispatch strategy was developed. A proposed solar plant with thermal storage is integrated to Heat Recovery Steam Generator (HRSG) considering several layout for different strategies either to supply heated water, saturated or superheated steam.

2. METHODS

2.1 Powerplant model

The reference power plant is composed of two 65 MW nominal gas turbines (GT), two Heat Recovery Steam Generators (HRSG) and one 62,5 MW nominal steam turbine (ST). Gas turbines operate with natural gas as fuel, and flue gas is the only heat source to the HRSG. The steam turbine is condensing type equipment, with one extraction to provide low-pressure steam to the deaerator. The HRSG is composed of the Low-Temperature Economizer (LTE), Economizer (ECO), a natural recirculation Evaporator (EVA) and two Superheater stages (SUP#1 and SUP#2), as represented in Figure 1. The power plant model was developed using the standard Modelica library ThermoSysPro, developed by EDF (El Hefni and Bouskela 2019), where some models were created or modified in order to represent specific plant conditions.

Some equipments were modeled on new condition with no loss of performance or degradation. Constant thermal losses from GT to ambient were applied, and for the remaining equipments thermal losses were assumed negligible. Constant isoentropic efficiency was used for modeling the GT and ST using reverse calibration (Hefni Baligh and Bouskela 2017). The HRSG model was built with dimensional and physical data, hence this approach allowed to evaluate the equipment's off-design performance, which is fundamental in the hybrid plant performance analysis. HRSG flue gas side physical properties factors and fin efficiency factor are applied according to The Babcock & Wilcox Company (2005). A PID control loop was applied for the level control on the drum.

2.2 Solar plant model

A solar plant model was built based on Andasol I and II plants (Al-Maliki et al. 2016; Llorente García, Álvarez, and Blanco 2011; NREL 2013), initially for validation purpose. This solar plant is composed of three main sections, as

depicted in Figure 2: the Solar Field (SF), the Thermal Energy Storage (TES) system, and the Power Block (PB). This model was later adapted to compose the hybrid plant model, by the replacement of the power block (section #3 on Figure 2) by the Heat Exchangers (HX) (section #4 on Figure 2) and reducing the scale of the SF and TES to meet the preselected hybrid plant thermal input.

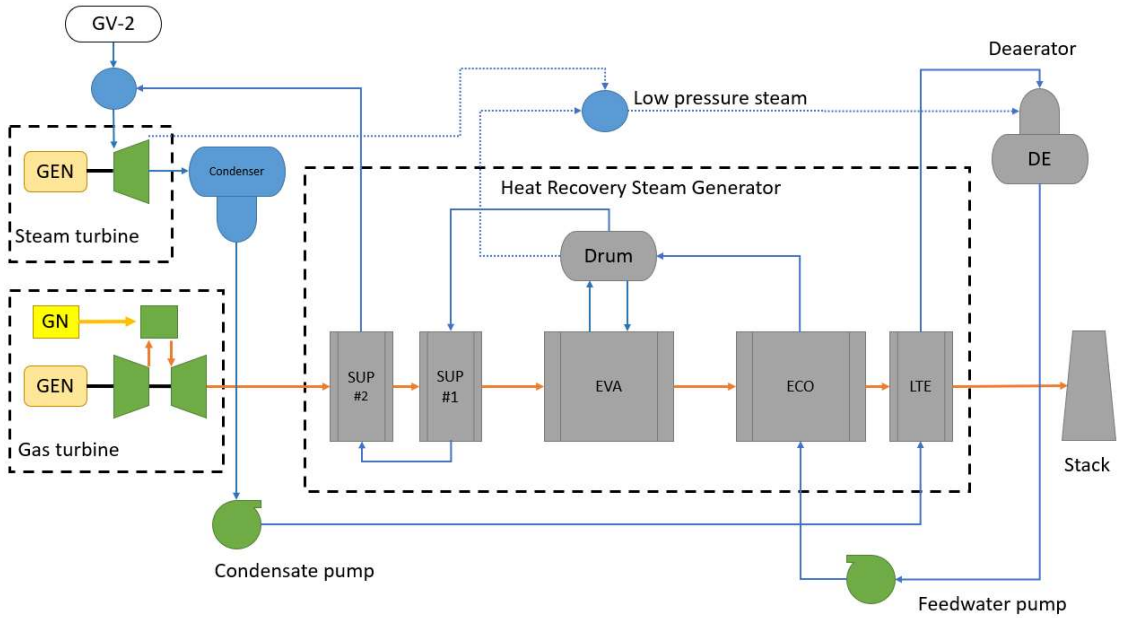

Figure 1. Reference combined cycle powerplant.

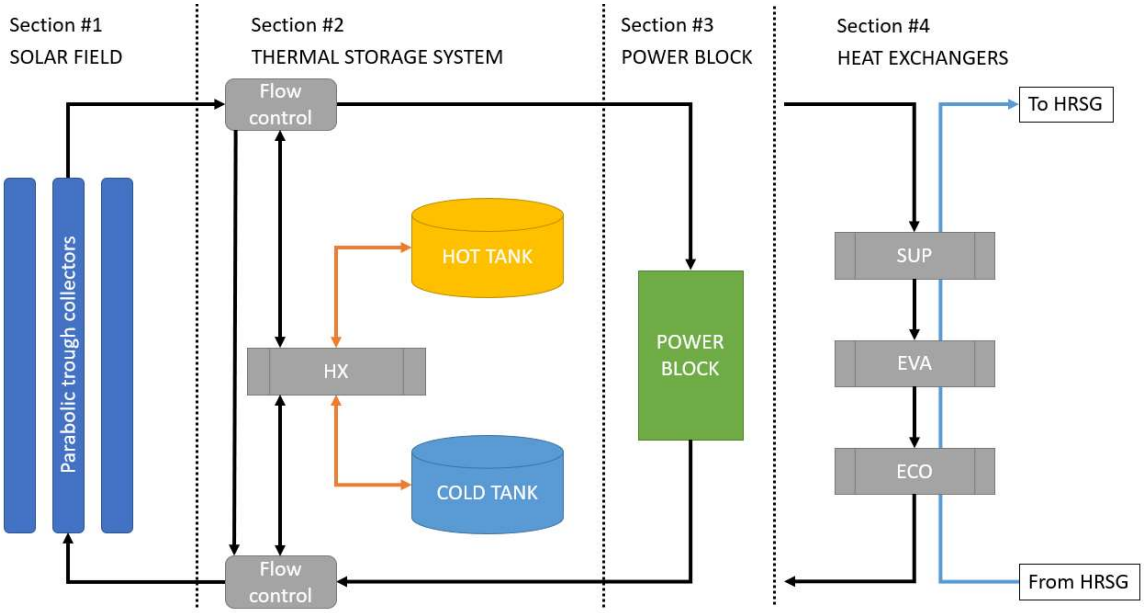

Figure 2. Solar plant flowchart with power block for validation.

The solar field section is composed of the parabolic trough collectors, main and recirculating HTP pumps, piping and headers. On the SF model, shown in Figure 3, boundary conditions (BC) were used to represent solar field inlet and outlet pressure, a control valve and a PID loop were applied to control the outlet HTF temperature, and a simple header model was used to account effects of piping thermal losses and thermal capacitance. The parabolic trough collector is the core of the solar field model, and it was further divided into three sections: external model, absorber tube wall and internal HTF flow. The external model formulation includes the optical model and thermal losses from absorber tube to ambient, as detailed in the sequence and shown in Figure 3. Tube wall and internal flow models were adapted from the ThermoSysPro library with minor adjustments to update fluid properties calculation; both models allow one-dimensional discretization.

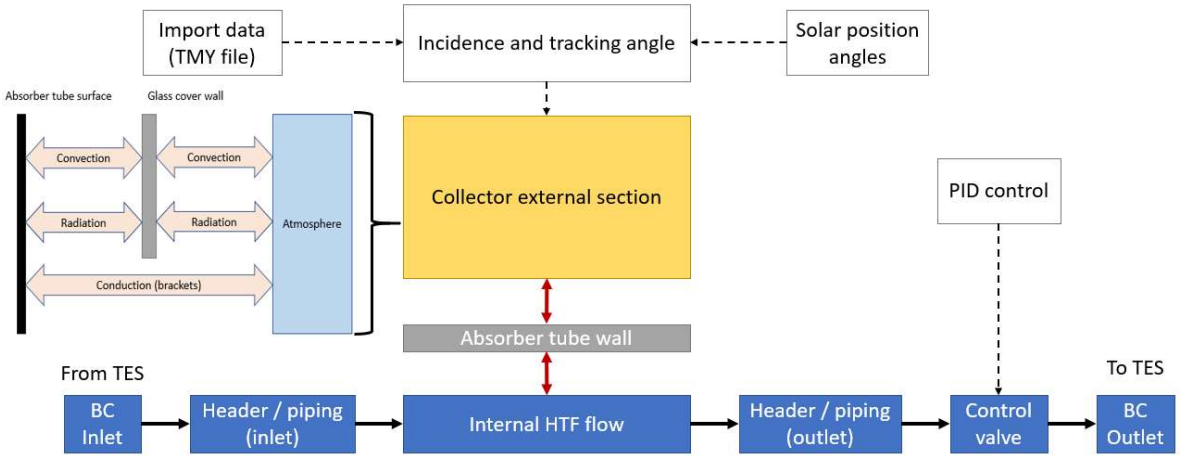

Figure 3. Solar field model with detail to the heat transfer modes included on the collector section.

On the external collector section, one-dimensional modeling was applied to model radiation, convection and conduction heat transfer, as proposed by Hefni and Bouskela (2019). Axial heat transfer on the collector assembly and radial conduction on the glass envelope were neglected, as proposed by Liang, You and Zhang (2015), while conduction losses on the brackets supports were considered assuming infinite length fin model. Equation (1) (Çengel 2007) was used for radiation heat transfer (W_{rad}) on the annulus and on the external side from the cover to the ambient, and Eq. (2) (Swinbank 1963) was used to account the sky temperature T_{sky}:

$$W_{rad} = \frac{A_1\,\sigma\,(T_1{}^4 - T_2{}^4)}{\frac{1}{\varepsilon_1} + \frac{D_1}{D_2}\left(\frac{1}{\varepsilon_2} - 1\right)}, \tag{1}$$

$$T_{sky} = 0{,}0552\,.\,T_{amb}^{1{,}5}\,, \tag{2}$$

Assuming the annulus is maintained with air at low pressure (below 0.013 Pa) convective heat transfer occurs mostly on the molecular level, therefore Ratzel, Hickox and Gartling (1978) correlation on Eq. (3) and (4) was applied. On the glass cover external surface, McAdams (1954) correlations adapted by Duffie and Beckman (2013) were used to obtain the Nusselt number on external forced convection considering wind influence, Eq. (5) and (6).

$$\gamma_{conv,r} = \frac{k_{gas}}{\frac{D_{r,o}}{2}\log\left(\frac{D_{g,i}}{D_{r,o}}\right) + \frac{b\,.\,\Lambda}{100}\left(\frac{D_{r,o}}{D_{g,i}} + 1\right)} \tag{3}$$

$$W_{conv,r} = A_{s\,.}\,\gamma_{conv,r}\,.\left(T_{r,o} - T_{g,i}\right) \tag{4}$$

$$Nu_{g,o} = 0{,}4 + 0{,}54.\,Re_{g,o}{}^{0{,}52} \tag{5}$$

$$Nu_{g,o} = 0{,}3.\,Re_{g,o}{}^{0{,}6} \tag{6}$$

where: $\gamma_{conv,r}$, k_{gas}, b, Λ are the convective heat transfer coefficient, gas thermal conductivity, interaction coefficient of annulus gas and mean-free-path between collisions of a molecule.

Equations (7) and (8) were applied for the energy balance on absorber tube and glass envelope nodes, and Eq. (9) for determining the amount of solar irradiation absorbed $W_{abs,r}$:

$$M_m\,.\,Cp_m\,.\frac{dT_m}{dt} = W_{abs,r} - W_{htf} - W_{rad,r} - W_{conv,r} - W_{cond,r} \tag{7}$$

$$M_g\,.\,Cp_g\,.\frac{dT_g}{dt} = W_{abs,g} + W_{rad,r} + W_{conv,r} - W_{rad,g} - W_{conv,g} \tag{8}$$

$$W_{abs,r} = N_{col}.A_{col}.\eta_{opt}.\varphi_{sun} \tag{9}$$

where: $W_{abs,r}$, W_{htf}, $W_{rad,r}$, $W_{conv,r}$, $W_{cond,r}$, are the powers absorbed on the tube surface, transferred to HTF, transferred by radiation and convection to the glass cover and transferred by conduction on the brackets to the ambient respectively, and M_m, Cp_m, $\frac{dT_m}{dt}$ are the metal section mass, thermal capacitance and temperature derivative. $W_{abs,g}$, $W_{rad,g}$, $W_{conv,g}$, are the solar power absorbed by the glass cover and radiative and convective thermal losses from cover to ambient respectively, and M_m, Cp_m, $\frac{dT_m}{dt}$ are the glass section mass, thermal capacitance and temperature derivative. On Eq. (9) N_{col}, A_{col}, η_{opt}, φ_{sun} are the number of collector rows in parallel, collector aperture area and optical efficiency, and solar Direct Normal Irradiance (DNI), respectively.

The optical efficiency was calculated with Eq. (10), according to (KALOGIROU 2014; Sodha, Mathur, and Malik 1984) and modified to account the shadowing effects between adjacent collector rows, as proposed by Sharma, Nayak and Kedare (2013) Eq. (11).

$$\eta_{opt} = \rho\,.\gamma.\tau_g.\alpha_r\left(1 - A_f.tan\,(\theta)\right).cos(\theta)\,.\eta_{IAM}.\,\eta_{shad} \tag{10}$$

$$\eta_{shad} = 1 - (1 - \frac{p}{w}\,cos\,(\beta)).(1 - \frac{p}{L}\,tan\,(\gamma_{col} - \gamma_{sol})) \tag{11}$$

where ρ, γ, τ_g, α_r, A_f, θ, η_{IAM}, η_{shad} are the mirror reflectivity, intercept factor, glass cover transmissivity, absorber tube absorptivity, geometric factor, incidence angle, incidence angle modifier and shadowing effect, respectively, and p, w, β, L, γ_{col}, γ_s are the row spacing, collector width, tracking angle and length, solar azimuth and collector azimuth.

The incidence angle and collectors tracking angle are given by Eq. (12) and (13) adapted from Duffie and Beckman (2013), while the remaining solar position angles were obtained using an existing model from the standard Modelica library SolarTherm.

$$cos(\theta) = \sqrt{cos^2(\theta_z) - cos^2(\delta).sen^2(\omega)} \tag{12}$$

$$tan(\beta) = tan(\theta_z)\,.sen(\gamma_{sol}) \tag{13}$$

where θ_z, δ, ω, are the zenith, solar declination, and solar hour angles, respectively.

The TES system is composed of a two-tank model (hot and cold tanks), which were adapted from the ThermoSysPro Modelica Library, the synthetic oil and molten salt heat exchanger and the control blocks, which were developed to control HTF flow among the solar field, storage system, heat exchangers and power block, under different operating conditions. Considering the complexity of concentrated solar plants, a simplified control model is proposed, as showed in Table 1. When the TES is fully charged, the solar field derate (mirror defocusing) may be necessary to keep the HFT temperature and flow under design limits; on the Modelica model this was performed on the control block by fixing the solar field mass flow rate at the power block design condition.

Table 1. Solar plant control strategy and cycle status.

Solar field		Flow output	Thermal energy (TES) available?	Cycle status	
0	Recirculation	-	No	0	Recirculation
1	Operation	$Q_{col} < Q_{proj}$		1	Partial load
		$Q_{col} \geq Q_{proj}$		2	Base load
		$Q_{col} < Q_{proj}$	Yes		
0	Recirculation	-		3	Recirculation & base load

A power block model was developed specifically for the solar plant validation and, therefore, an analogous approach to the SAM software was adopted to reduce the effect of this component over validation analysis. A correction factor was applied to the power block thermal-to-electric conversion as a function of the thermopower input, as proposed by Llorente García, Álvarez and Blanco (2011), and the HTF outlet temperature is assumed constant. Parasitic consumptions for each solar plant section were estimated from the Andasol 3 plant (Ramorakane and Dinter 2016),

including HTF main and recirculating pumps and TES pump, and also corrections were applied for off-design conditions using pump affinity laws. Parasitic loads were used to estimate the solar plant net power output.

Heat exchangers modeling was performed by means of Effectiveness-NTU method (Çengel 2007), considering counter-flow shell and tube exchangers. Equation (14) is applied to correct the off-design performance, as proposed by (Patnode 2006).

$$\frac{UA}{UA_{des}} = \left(\frac{\mathrm{Q}_{htf}}{\mathrm{Q}_{htf\_des}}\right)^{0,8} \tag{14}$$

where: UA_{des} and UA are the heat transfer coefficient and area product at design and off-design conditions respectively, and Q_{htf_des} and Q_{htf} are the mass flow rate at design and off-design conditions.

2.3 Solar plant sizing and hybrid configurations

The solar plant was sized to provide approximately 2% increasing in ST power output, with the main parameters shown in Table 2. The TES system was oversized with the purpose to avoid the influence of this section on the solar plant performance hence no derate condition is considered on the solar field while keeping the nominal HTF mass flow rate to the heat exchangers. The heat exchangers configurations and sizing were adjusted for each layout to achieve the selected HTF and steam outlet temperatures on nominal conditions.

Table 2. Solar plant parameters.

Parameter	Dimensions
Number of collector rows in parallel	4
Solar field aperture area, m²	13080
HTF inlet temperature (synthetic oil), °C	293 -303
HTF outlet temperature (synthetic oil), °C	393
Nominal mass flow rate (synthetic oil), kg/s	30
HTF inlet temperature (molten salt), °C	293
HTF outlet temperature (molten salt), °C	520
Nominal mass flow rate (molten salt), kg/s	20.67

The solar plant was connected to the reference plant considering 9 layouts, as detailed in Table 3. Molten salt was used on layouts #7 and 8# to achieve the nominal HRSG outlet steam temperature since synthetic oil temperature must be controlled under 400 °C to avoid thermal degradation. It was assumed fixed inlet water temperature on both solar and reference plant, as showed in Table 3. A single day was chosen for the analysis, January-15th, when nominal Direct Normal Irradiance (DNI) is available. The solar-to-electric efficiency (η_{solar}) (Behar 2018), the average ST additional power (W_{st-ad}), the HRSG efficiency (η_{hrsg}) and the fuel saving potential (Q_{saved}) were used as parameters to evaluate the performance of each layout, according to equations (15) to (18), respectively.

Table 3. Hybrid layouts configuration.

No #	HTF	Extraction point	T_e (°C)	Return point	T_r (°C)
#1	Oil	CP outlet (condensate)	54	Drum (heated water)	280
#2	Oil	CP outlet (condensate)	54	Drum (saturated steam)	292
#3	Oil	CP outlet (condensate)	54	SUP#1 outlet (superheated steam)	380
#4	Oil	Drum (saturated liquid)	288	Drum (saturated steam)	292
#5	Oil	Drum (saturated liquid)	288	SUP#1 outlet (superheated steam)	380
#6	Oil	Drum (saturated steam)	290	SUP#1 outlet (superheated steam)	380
#7	Molten Salt	Drum (saturated liquid)	288	SUP#2 outlet (superheated steam)	500
#8	Molten Salt	Drum (saturated steam)	290	SUP#2 outlet (superheated steam)	500
#9	Oil	CP outlet (condensate)	54	Deaerator (low pressure steam)	116

$$\eta_{solar} = \frac{W_{net} - W_{ref}}{Q_{solar}} \tag{15}$$

$$W_{st-ad} = \frac{W_{st} - W_{st\_ref}}{W_{st-ref}} \tag{16}$$

$$\eta_{hrsg} = \frac{h_{out\_tg} - h_{out\_hrsg}}{h_{out\_tg} - h_{in\_tg}} \tag{17}$$

$$Q_{saved} = \frac{24.(W_{net} - W_{ref})}{\eta_{fuel\_ref}} \quad (18)$$

where: W_{net}, W_{ref}, Q_{solar}, W_{st}, W_{st_ref} are the daily averaged values for the plant net power, the reference plant net power, the thermopower provided by the solar field, the ST gross power and ST gross power on the reference plant, respectively, h_{in_tg}, h_{out_tg}, h_{out_hrsg} are the flue gas enthalpy values on the GT inlet, exhaust and HRSG outlet respectively, and η_{fuel_ref} is the reference plant fuel-to-electric energy conversion efficiency.

3. MODEL VALIDATION

The reference powerplant simulation was performed on nominal meteorological site conditions, and the operational data was collected on the first months of each subsystem to minimize degradation and loss of performance influence. The results obtained with the Modelica model showed good agreement with operational data as disposed on Table 4, with differences up to 3%. Part of the differences is because the steam turbine and the HRSG were commissioned about 8 years after the gas turbines, thus: (1) when gas turbine power and output temperature reference data was collected the GT operated on open cycle, therefore the exhaust backpressure was lower and (2) when steam turbine power and HRSG mass flow reference data was collected the GT efficiency was reduced, therefore increased GT exhaust energy was available to the HRSG.

Table 4. Comparison between simulation and reference.

Gas Turbine	**Reference**	**Simulation**	**Difference**
Generator Power Output, MWe	64,18	63,15	-1,60%
Flue Gas Outlet Temperature, °C	600,4	605	0,53%
Steam Turbine			
Generator Power Output, MWe	62,17	60,8	-2,20%
Steam Temperature, °C	47,5	54,17	2,08%
Heat Recovery Steam Generator			
Steam Mass Flow, kg/s	29,7	29,0	-2,59%
Drum Pressure, MPa	75,85	74,24	-2,12%
Condensate Inlet Temperature, °C	56,2	54,1	-0,64%
Feedwater Inlet Temperature, °C	102,9	102,9	0,00%
Steam Outlet Temperature, °C	505	502,3	-0,35%
Flue Gas Outlet Temperature, °C	184,4	185,2	0,17%

The validation of the solar plant was performed on the month of January, using a Typical Meteorological Year (TMY) file for the reference power plant location. The comparison of the solar field power transferred to the HTF obtained by Modelica and SAM models is shown in Figure 4, for three selected days representing approximately 100%, 65% and 35% of nominal DNI. Higher deviance is noted at the beginning of each day (note 1) due to strong transient behavior during the solar field initialization. In general, the difference from Modelica to SAM models is below 2%. On January-15th, TES system is not able to store all available solar energy, hence solar field derate is applied (note 2) and the mass flow is controlled to meet the power block design requirements.

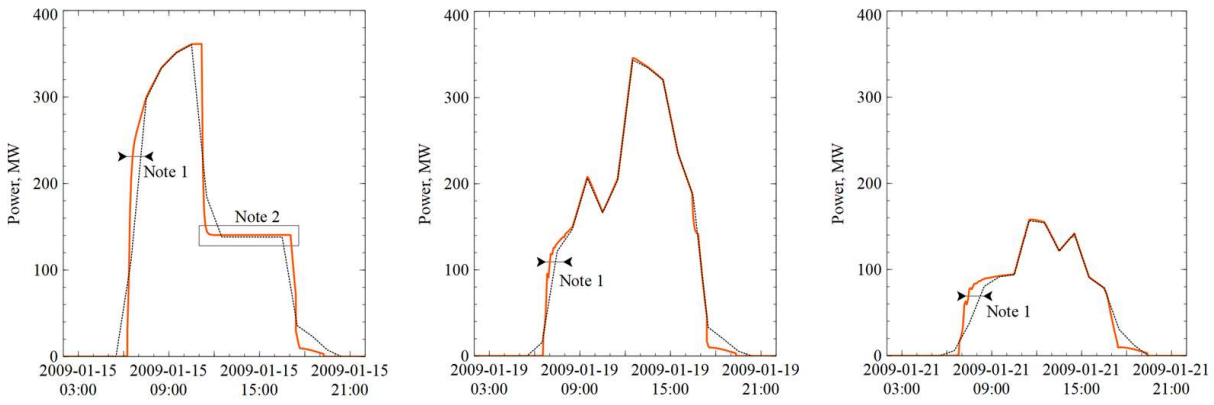

Figure 4. Comparison between the results for the present modeling in Modelica software (solid lines) and SAM (dot lines) simulation for the thermopower transferred to HTF on selected days: January-15th, January-19th and January-21st.

The temperature at the inlet of the power block, the power block gross power and the solar plant net power are shown in figure 5, for January-15th. Under steady-state condition, the Modelica solar plant model exhibits good agreement with SAM, although a higher difference is noted during initialization, TES modulation and shutdown.

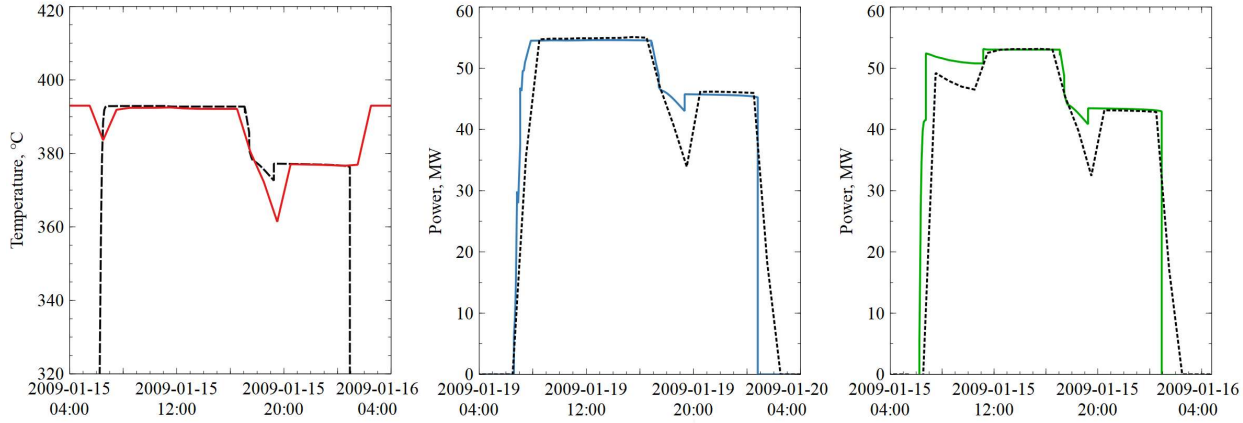

Figure 5. Comparison between the Modelica (solid lines) and SAM (dot lines) simulation results on jan-15th, from left to right: power block HTF inlet temperature, power block gross power and solar plant net power.

4. RESULTS AND DISCUSSION

The performance indicators for each layout investigated are presented in Table 5, where E_{solar} and E_{par} are the amount of thermal energy provided by the SF to the TES system and the solar plant-parasitic consumption on January-15th, respectively. E_{solar} lower values are verified on layouts #7 and #8, where molten salt is used as HTF and the receiver average temperature is higher, thus implying higher thermal losses. Nonetheless, parasitic consumption tends to be lower on these layouts since the higher temperature range for molten salt results reduced mass flow on the solar field and TES, reducing pumps power consumption. Solar-to-electric efficiency is also higher for layout #7 and #8 since the solar energy is transferred to the Rankine cycle at higher temperatures.

Table 5. Main performance indicators values for each hybrid layout.

Layout	E_{solar} (MW-h)	E_{par} (MW-h)	η_{solar}	W_{st-ad}	Q_{saved} (MW-h)
#1	44.840	0.610	14.63%	0.47%	13.859
#2	44.821	1.179	31.57%	1.02%	29.894
#3	44.762	1.217	33.00%	1.07%	31.204
#4	44.791	1.719	41.74%	1.36%	39.697
#5	44.804	1.610	41.95%	1.38%	39.507
#6	44.737	1.671	43.23%	1.42%	40.859
#7	42.292	1.102	43.98%	1.33%	39.296
#8	42.112	1.038	47.21%	1.41%	42.000
#9	44.889	1.264	10.23%	0.38%	9.697

Overall, the performance of layouts #4 to 8# are similar, with average differences up to 0.05 MW on steam turbine and 7% on fuel saved energy. For these layouts, the use of solar energy to evaporate saturated water and/or superheat steam enables a larger mass flow rate on HRSG, therefore improving its efficiency, as shown in Figure 6 on the left, and by the exhaust flue gas temperature in the HRSG outlet (T_{stack}) in Table 6. The steam turbine gross power curves of each layout and the base plant are shown on Figure 6 on the right.

Some control variables are presented in Table 6, with respective variations relative to the reference plant, and measurements taken at January-15th 12:00 on steady-state conditions. The ECO outlet temperature T_{eco} must be controlled to prevent steaming and damage to the ECO tubes, although on most layouts this temperature tends to fall with the increase of the HRSG flow rate. The steam temperature of the HRSG outlet (T_{steam}) changes from -3.4 to +8.3 °C in relation to the base plant: values below 492 °C should be avoided to prevent steam condensation and blades erosion on ST final stages, while temperatures higher than 508°C should be further investigated, regarding metallurgical design limits on SUP#2 tubes and ST, hence a desuperheater stage should be provided for layouts #7 and #8. Finally, the last column in Table 6 presents the instantaneous power output on ST (W_{st}), which is a principal restriction to the solar field size since the steam turbine output should be maintained under 64 MW as a design limitation.

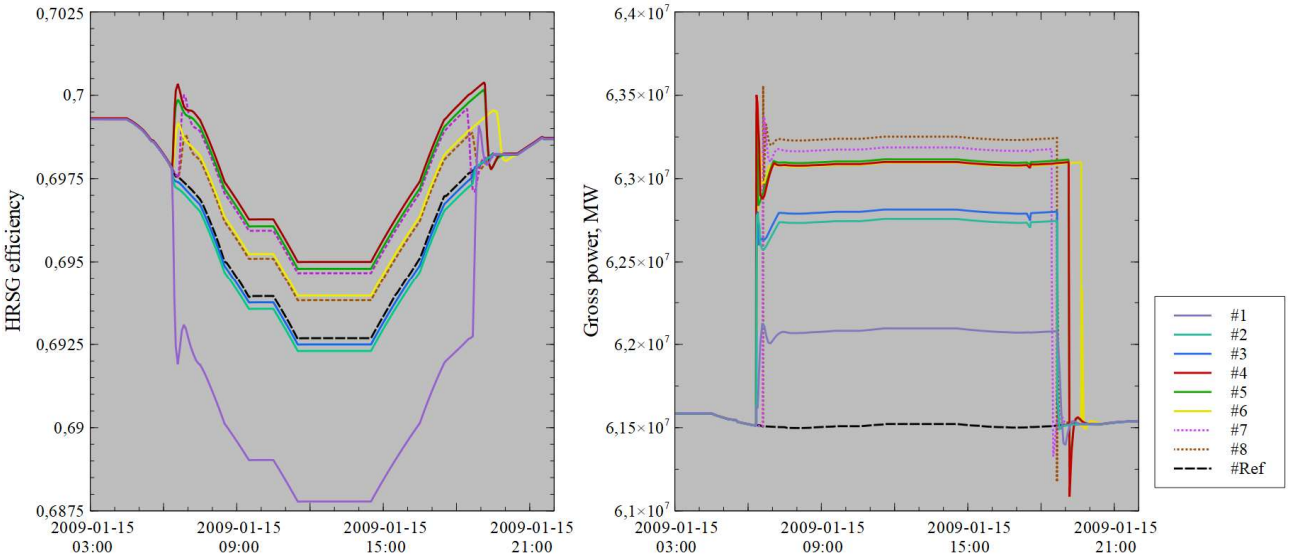

Figure 6. HRSG efficiency (on the left) and the steam turbine power increase (on the right) for each layout, with reference to the base plant.

Table 6. Additional parameters measured at January-15 12:00 under steady-state condition.

	T_{stack}, °C		T_{eco}, °C		T_{steam}, °C		Q_{hrsg}, kg/s		W_{st}, MWe	
Layout	Val.	Dif.	Val.	Dif.	Val.	Dif.	Val.	Dif.	Val.	Dif.
Ref. Plant	184.6		275.5		508.2		29.1		61.5	
#1	187.8	3.2	279.0	3.4	507.0	-1.2	29.4	1.0%	62.1	0.9%
#2	184.9	0.3	275.8	0.3	505.6	-2.7	29.7	2.1%	62.8	2.0%
#3	184.8	0.2	275.7	0.1	506.5	-1.7	29.7	2.0%	62.8	2.1%
#4	183.1	-1.5	273.8	-1.7	504.8	-3.4	29.8	2.6%	63.1	2.6%
#5	183.3	-1.3	274.0	-1.5	506.4	-1.9	29.8	2.5%	63.1	2.6%
#6	183.8	-0.8	274.7	-0.8	512.5	4.2	29.6	1.8%	63.1	2.6%
#7	183.3	-1.3	274.1	-1.4	508.5	0.3	29.8	2.3%	63.2	2.7%
#8	183.9	-0.7	274.7	-0.8	516.5	8.3	29.5	1.5%	63.3	2.8%
#9	184.6	0.0	276.3	0.8	508.2	0.0	29.1	0.0%	61.9	0.6%

5. CONCLUSION

A reference power plant in Brazil was modeled and validated through real operational data and a solar plant model with synthetic oil and molten salt as working fluids was created and validated with the reference software SAM. The reference plant and solar plant models were used to simulate and analyze the thermodynamic performance of nine different hybrid plant configurations, considering bottoming level hybridization. Results showed the layouts that use solar energy to evaporate the saturated liquid and/or superheat steam have the best thermodynamic performance, including synthetic oil and molten salt alternatives. Molten salt layouts presented higher thermal losses on the solar field due to higher operating temperature, although compensated by a higher solar-to-electric energy conversion efficiency and lower parasitic consumption.

Finally, the hybrid power plant is a efficient option to convert solar thermal energy into electric energy, with efficiency up to 47,21%, while it enables to increase the HRSG efficiency up to 0,23%, therefore hybridization is an advantageous alternative for both the solar plant and the combined cycle plant. Moreover, the integration of solar thermal energy with the base Rankine cycle has the potential to to reduce fossil fuel consumption up to 42 MW-h/day, which represents around 0,45% from daily fossil fuel comsumption, hence it is a promising alternative to be considered on retrofitting evaluation of existing powerplants and for projects of new facilities.

6. REFERENCES

Abdelhalim, Adham M., and Inés M. Suárez-Ramón. 2020. “Potential Fuel Savings in a Combined Cycle in Egypt by Integrating a Parabolic Trough Solar Power Plant.” *Renewable Energy and Power Quality Journal* 18(18): 333–38.

Al-Maliki, Wisam Abed Kattea, Falah Alobaid, Vitali Kez, and Bernd Epple. 2016. “Modelling and Dynamic Simulation of a Parabolic Trough Power Plant.” *Journal of Process Control* 39: 123–38.

Antonanzas, J., M. Alia-Martinez, F. J. Martinez-De-Pison, and F. Antonanzas-Torres. 2015. “Towards the Hybridization of Gas-Fired Power Plants: A Case Study of Algeria.” *Renewable and Sustainable Energy Reviews* 51: 116–24.

Behar, Omar. 2018. “Solar Thermal Power Plants - A Review of Configurations and Performance Comparison.” *Renewable and Sustainable Energy Reviews* 92: 608–27.

Boretti, Albert, and Sarim Al-Zubaidy. 2019. “A Case Study on Combined Cycle Power Plant Integrated with Solar Energy in Trinidad and Tobago.” *Sustainable Energy Technologies and Assessments* 32: 100–110.

Burin, Eduardo, Pedro Lo Giudice, and Edson Bazzo. 2018. “Paper Mill Cogeneration Power Plant Assisted by Linear Fresnel Solar Collectors.” *O Papel* 79(5): 86–89.

Burin, Eduardo Konrad et al. 2015. “Boosting Power Output of a Sugarcane Bagasse Cogeneration Plant Using Parabolic Trough Collectors in a Feedwater Heating Scheme.” *Applied Energy* 154: 232–41.

Burin, Eduardo Konrad et al.. 2016. “Thermodynamic and Economic Evaluation of a Solar Aided Sugarcane Bagasse Cogeneration Power Plant.” *Energy* 117: 416–28.

Çengel, Y. A. 2007. 18 Biotechnology Letters *Heat and Mass Transfer. A Practical Approach*. Third Edit. McGraw-Hill.

Duffie, J. A., and William A. Beckman. 2013. 9 Clinics in Laboratory Medicine *Solar Engineering of Thermal Processes*. Fourth Edi. Hoboken, New Jersey: John Wiley & Sons, Inc.

Elmohlawy, Ashraf E., Valery F. Ochkov, and Boris I. Kazandzhan. 2019. “Thermal Performance Analysis of a Concentrated Solar Power System (CSP) Integrated with Natural Gas Combined Cycle (NGCC) Power Plant.” *Case Studies in Thermal Engineering* 14: 100458.

Hefni Baligh, El, and Daniel Bouskela. 2017. “Modeling and Simulation of Complex ThermoSysPro Model with OpenModelica - Dynamic Modeling of a Combined Cycle Power Plant.” *Proceedings of the 12th International Modelica Conference, Prague, Czech Republic, May 15-17, 2017* 132: 407–14.

El Hefni, Baligh, and Daniel Bouskela. 2019. Modeling and Simulation of Thermal Power Plants with ThermoSysPro *Modeling and Simulation of Thermal Power Plants*.

Hefni, Baligh El, and Daniel Bouskela. 2019. *Modeling and Simulation of Thermal Power Plants with ThermoSysPro*. 1ª. Chatou, France: Springer Nature Switzerland AG.

KALOGIROU, S. A. 2014. Elsevier Inc. *Solar Energy Engineering, Processes and Systems*. Second Edi. Elsevier Inc.

Liang, Hongbo, Shijun You, and Huan Zhang. 2015. “Comparison of Different Heat Transfer Models for Parabolic Trough Solar Collectors.” *Applied Energy* 148: 105–14.

Llorente García, Isabel, José Luis Álvarez, and Daniel Blanco. 2011. “Performance Model for Parabolic Trough Solar Thermal Power Plants with Thermal Storage: Comparison to Operating Plant Data.” *Solar Energy* 85(10): 2443–60.

Manente, Giovanni. 2016. “High Performance Integrated Solar Combined Cycles with Minimum Modifications to the Combined Cycle Power Plant Design.” *Energy Conversion and Management* 111: 186–97.

Manente, Giovanni, Sergio Rech, and Andrea Lazzaretto. 2016. “Optimum Choice and Placement of Concentrating Solar Power Technologies in Integrated Solar Combined Cycle Systems.” *Renewable Energy* 96: 172–89.

McAdams, W. H. 1954. “No Title.” In *Heat Transmission*, New York: McGraw-Hill.

NREL. 2013. *System Advisor Model (SAM) Case Study: Andasol-1*. https://sam.nrel.gov/images/web_page_files/sam_case_csp_physical_trough_andasol-1_2013-1-15.pdf.

Patnode, A. M. 2006. 1 “Simulation and Performance Evaluation of Parabolic Trough Solar Power Systems.” University of Wisconsin- Madison.

Peterseim, Juergen H., Stuart White, Amir Tadros, and Udo Hellwig. 2014. “Concentrating Solar Power Hybrid Plants - Enabling Cost Effective Synergies.” *Renewable Energy* 67: 178–85.

Powell, Kody M. et al. 2017. “Hybrid Concentrated Solar Thermal Power Systems: A Review.” *Renewable and Sustainable Energy Reviews* 80: 215–37.

Pramanik, Santanu, and R. V. Ravikrishna. 2017. “A Review of Concentrated Solar Power Hybrid Technologies.” *Applied Thermal Engineering* 127: 602–37.

Ramorakane, Relebohile John, and Frank Dinter. 2016. “Evaluation of Parasitic Consumption for a CSP Plant.” *AIP Conference Proceedings* 1734(May 2016): 1–9.

Ratzel, A.C., C.E. Hickox, and D.K. Gartling. 1978. “Energy Loss by Thermal Conduction and Natural Convection in Annular Solar Receivers.” In *Thermal Conductivity*, Boston, MA: Springer, 423–32.

Sharma, V. M., J. K. Nayak, and S. B. Kedare. 2013. “Shading and Available Energy in a Parabolic Trough Concentrator Field.” *Solar Energy* 90: 144–53.

Sodha, M.S., S.S. Mathur, and M.A.S. Malik. 1984. “Solar Concentrators.” In *Reviews of Renewable Energy Resources*, New Delhi: Wiley Eastern Ltd.

Soria, Rafael et al. 2015. “Hybrid Concentrated Solar Power (CSP)-Biomass Plants in a Semiarid Region: A Strategy for CSP Deployment in Brazil.” *Energy Policy* 86: 57–72.

Swinbank, W.C. 1963. “Longwave Radiation from Clear Skies.” *Q.J.R. Meteor. Soc.* 89: 339–48.

The Babcock & Wilcox Company. 2005. *Steam Its Generation and Use*. 41st ed. eds. John B. Kitto and Steven C. Stultz. Barberton, Ohio: The Babcock & Wilcox Company.

7. RESPONSIBILITY NOTICE

The authors are the only responsible for the printed material included in this paper.